Term Project Report of 2.094

# Ductile Fracture Characterization of an Aluminum Alloy Sheet using Numerical Simulations and Tests

By

Meng Luo

**Impact and Crashworthiness Lab**
**Department of Mechanical Engineering**
**Massachusetts Institute of Technology**

Apr 28, 2008

# Contents

## Abstract

The objective of this project is to characterize the plastic behavior and ductile fracture of the 2mm-thick aluminum alloy sheets. Four different types of tests were conducted all the way to fracture, including tensile tests on classical dog-bone specimens, flat specimens with cutouts and plane strain grooved specimens, as well as a punch indentation test. A comprehensive numerical analysis of these experiments was performed with ADINA. Simulations revealed that the isotropic plasticity model is able to describe, with good accuracy, the plastic response of all four types of tests. Moreover, local equivalent strain to fracture and stress triaxiality parameters were obtained through FE simulations using an inverse engineering method, and a fracture locus of this type of aluminum alloy sheets was determined. In addition, a parametric study was performed to evaluate the effect some variables that will affect numerical simulations, such as number of integration points through thickness, element type, and mesh size.


## 1. Introduction

Prediction of ductile fractures of metals in engineering structures is a topic of great importance in the automotive, aerospace, and military industries. Equivalent strain to fracture $\bar{\varepsilon}_f$ (or the fracture strain for short) is widely used to define the material ductility. Many theoretical analyses and experimental results have shown that the material's fracture strain is not constant but changes under different loading conditions or stress states. The most important fracture controlling parameter is the stress triaxiality $\eta$ (normalized hydrostatic pressure by Mises equivalent stress, $\frac{\sigma_m}{\bar{\sigma}} = -\frac{p}{\bar{\sigma}}$).

Based on the research experience of ICL(Impact and Crashworthiness Lab) at MIT, a Mohr-Coulomb fracture criterion in the space of $\bar{\varepsilon}_f$ and $\eta$ was adopted in this project to determine the fracture locus of the aluminum sheets. For sheet metal, the stress triaxiality range of most interest is $1/3 < \eta < 2/3$. Therefore, four types of tests which can cover this range were designed to calibrate the fracture model.

The present approaches include experimental study and FE simulation. Experiments will provide the load-displacement response, the location and position of fracture initiation. FE simulations are used to calculate all the stress states and strain components at the point of fracture initiation.

Besides the fracture calibration, a parametric study based on the ADINA simulations of the calibration tests was conducted to evaluate the effect of several important finite element parameters.

# 2. Numerical Simulations of Four Fracture Calibration Test

Four different types of tests which can cover different stress triaxialities were conducted on a MTS uniaxial testing machine. All four types of specimens were cut from the 2mm-thick aluminum sheet. The analytical triaxialities for the four types of tests are: 1/3(dog-bone specimen), 0.52(flat specimen with cutout), 0.577(plane strain specimen) and 2/3(punch indentation). Corresponding numerical simulations were performed to predict to load displacement responses and obtain local stress states and strain components. All the numerical simulations of this project were run in the environment of ADINA V.8.4.4, and within ADINA structures and statics.

Fig. 2-1 MTS testing machine

## 2.1 Dog-bone tensile specimens

### 2.1.1 Obtaining hardening rule and quantification of anisotropy

Uniaixal tensile tests on the dog-bone specimens cut from the aluminum sheets are very important, since the material data needed for the FE simulations are usually obtained by these tests. Nine dog-bone specimens were cut using water-jet machining, three from each of the following directions :(angle between the tensile direction and the material rolling direction): $0^o$, $45^o$, and $90^o$, as is shown in Fig. 2-2.

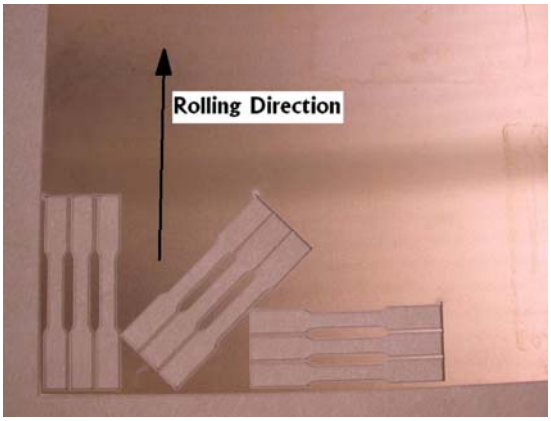


Fig. 2-2 Original sheet of from which specimens were machined

Force versus displacement was recorded during each of the 12 uniaxial tension tests. The recorded force-displacement data in three directions is shown in Fig. 2-3. The onset of diffuse necking is indicated for each test. The calculated engineering stress-strain curve up to necking is given in Fig. 2-4.

It is clear that the load-displacement curves are the same in all three directions up to the point of necking. This means that sheets exhibit planar anisotropy. The corresponding true stress versus the equivalent plastic strain up to the necking strain is shown in Fig. 2-5.

In order to extend the range of strain and avoid tensile instability, a simple power law fitting of the true stress strain curve was used in this project. Comparison of the true stress-true strain curves with the power law fit is shown in Fig. 2-6. The form of the power law fitting is:

$$\overline{\sigma} = A(e_0 + \overline{\varepsilon}_p)^n \tag{2-1}$$

Using least square method, the parameters of the power law fitting are:

$$A = 438MPa, e_0 = 0.00434, n = 0.07$$

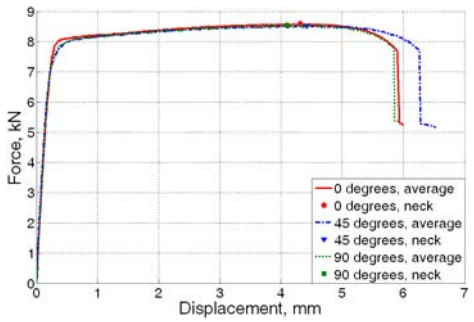


Fig. 2-3 Force versus displacement curves measured for dog-bone specimens

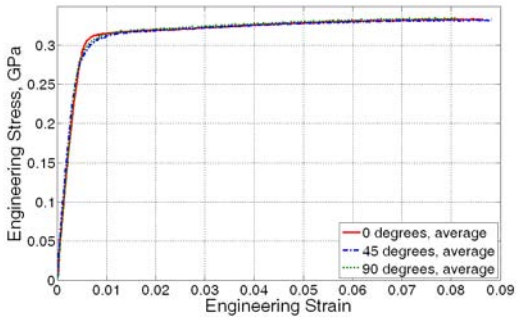


Fig 2-4 Engineering stress strain curves up to necking for dog-bone specimens

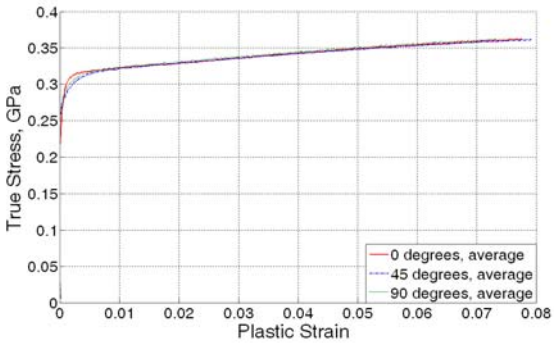


Fig. 2-5 True stress versus plastic strain calculated up to necking for dog-bone specimen uniaxial tension tests

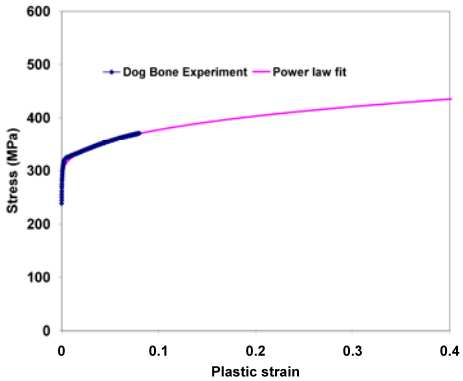


Fig. 2-6 True stress-strain curve obtained from dog-bone specimen tension tests and the power hardening fit

The true stress strain relation in Fig. 2-6 can be used for the material input of ADINA. However, aluminum sheets are known to develop considerable anisotropy during the extrusion and rolling processes and subsequent heat treatment. Although Fig. 2-3~2-5 indicate that this sheet are planar anisotropic, one still need to quantify the anisotropy of this material, especially the transverse (through thickness) anisotropy. Since the plastic orthotropic material in ADINA is a good choice to represent the transverse anisotropic material, several measurements were taken to obtain the Lankford parameter needed for the orthotropic material model.

This parameter, referred to as "$r_\alpha$," is the ratio of the strain in the width direction, $d\varepsilon_{\alpha+\pi/2}$, to the strain through the thickness direction, $d\varepsilon_3$, of a specimen subjected to uniaxial tension in the direction defined by the angle $\alpha$ measured from the rolling direction.

$$r_\alpha = \frac{d\varepsilon_{\alpha+\pi/2}}{d\varepsilon_3} \tag{2-2}$$

The Lankford parameter in three directions was measured using Digital Image Correlation, as shown in Fig. 2-7. The calculated values of the Lankford parameters are given in Table 2-1. Herein, all the material data needed for both the isotropic and an orthotropic material model in ADINA have been obtained from tests.

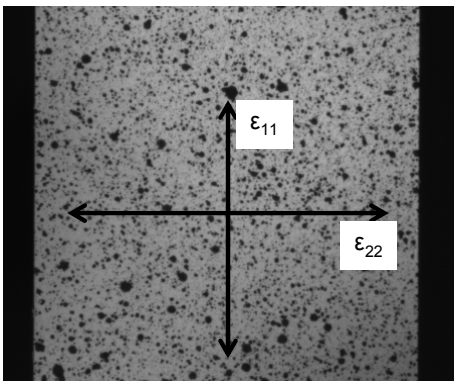


Fig. 2-7 Measuring lankford parameters with Digital image correlation

Table 2-1 Measured value of the Lankford parameters for our aluminum sheet

| $r_0 = r_x$ | $r_{45}$ | $r_{90} = r_y$ |
|---|---|---|
| 0.638 | 0.6 | 0.7 |

### 2.1.2 Numerical simulations of dog-bone specimen tensile test

In order to find the best numerical model for the series of tests, total four FE models of the dog-bone tension tests were built in ADINA, two with 4-node shell elements, the other two with 8-node solid elements. For each element type, both isotropic and orthotropic plasticity model were used. Since the specimen is symmetric with respect to all three axes, only a 1/8 model was built with solid elements, and a quarter model was built with shell elements. The top of the specimen is subjected to a prescribed displacement, and symmetric boundary conditions are set on corresponding edges (lines for shell, surfaces for solid elements). The models are shown in figure 2-8~2-11.

The elastic material parameters used in the models are:E=69Gpa, density=2700kg/m$^3$, poisson ratio=0.33. The plastic stress strain curve used for both isotropic and orthotropic material model is the one in Fig. 2-6. The lankford parameters for orthotropic material model are shown in table 2-1. Since the aluminum sheet is almost planar isotropic, and our objective is to investigate the difference between orthotropic and isotropic material model, the material a direction (rolling direction) was simply set to along with the tension direction for orthotropic material model (Fig. 2-9, 2-11). The mesh edge length is about 1mm, and the number of though thickness integration points is set to 5 for shell model.

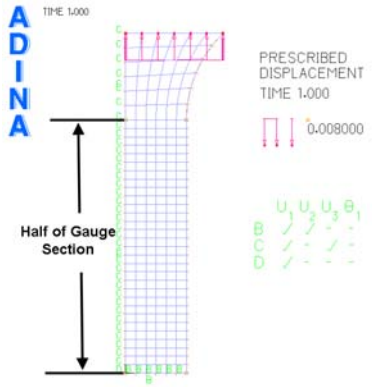


Fig 2-8 Model 1: Shell element with isotropic material model

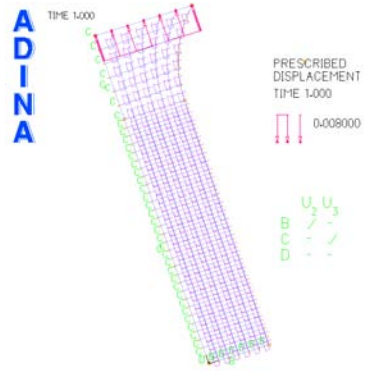


Fig 2-9 Model 2:Shell element with orthotropic material model

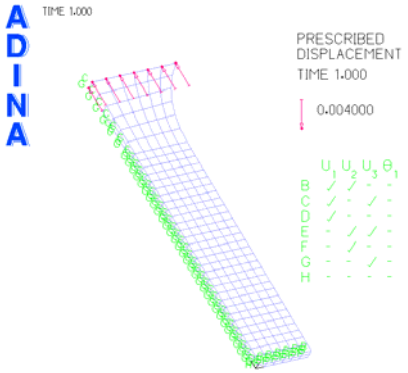


Fig 2-10 Model 3: Solid element with isotropic material model

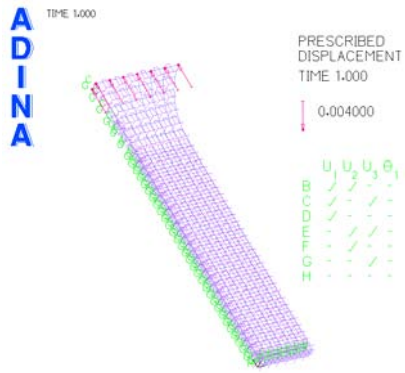


Fig 2-11 Model 4: Solid element with orthotropic material model

To obtain the force-displacement response, a time function is defined for the prescribed displacement, and the time step is 0.01s. The analysis assumptions are large displacement and strain, and a full Newton method was used for iteration. All the models are run in the environment of ADINA statics hereafter in this report.

Fig. 2-3 shows that the average gauge section elongation to fracture is 6.1mm. The corresponding deformation shape and effective plastic strain band plot at the fracture point are shown in Fig. 2-12~2-15. The deformation figures shows that only model 3, which is with isotropic material model and solid elements, can predict the necking phenomenon before fracture, see Fig. 2.16.

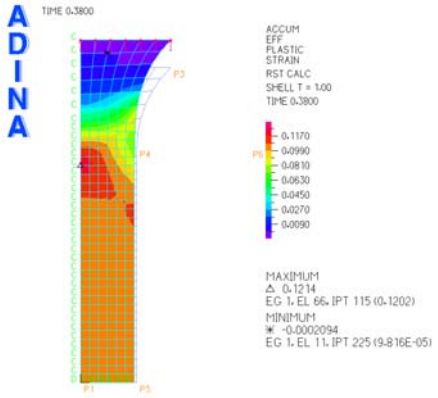


Fig 2-12 Deformation and strain output of model 1

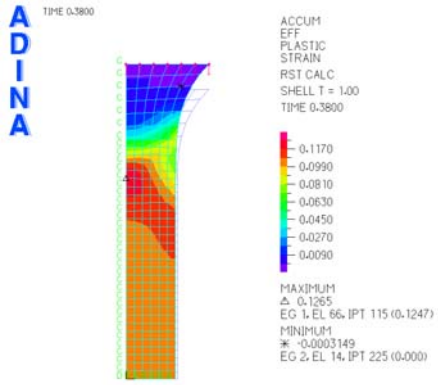


Fig 2-13 Deformation and strain output of model 2

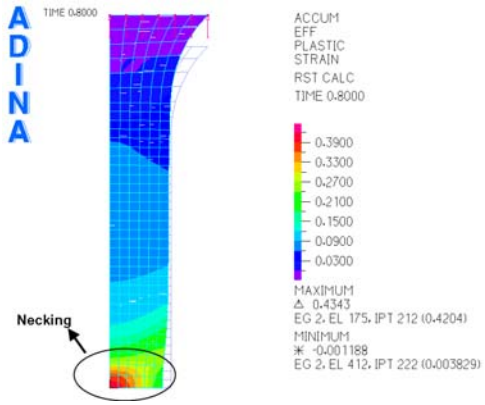


Fig 2-14 Deformation and strain output of model 3

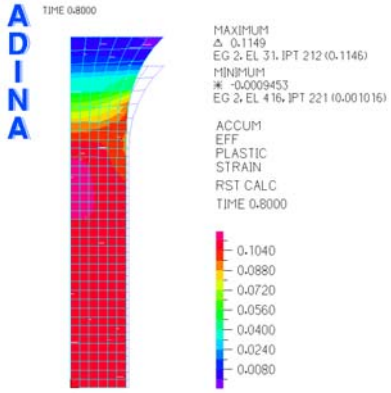


Fig 2-15 Deformation and strain output of model 4

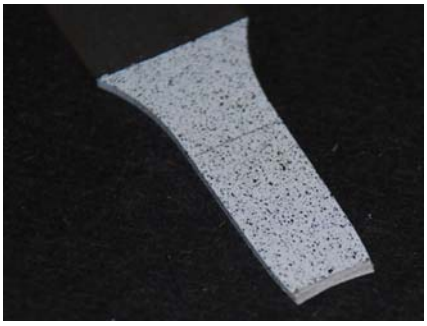

Fig 2-16 Necking occurs in tensile tests

From the simulation result, the total reaction force of the top nodes and the gauge

nodes displacement can be obtained. The load displacement responses and the experimental results were compared in Fig 2-17. Apparently, the model 3 result accords with experimental result very well.

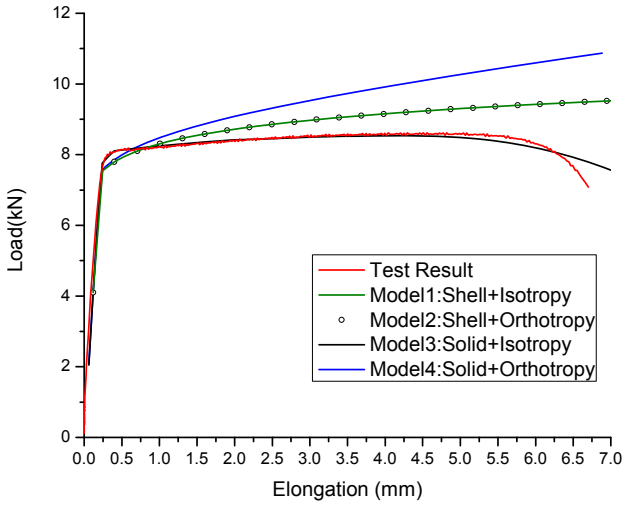


Fig. 2-17 Comparison of load-displacement curves between experiment and simulations

Previous research of ICL shows that the crack initiates at the center of the dog-bone specimen in a tensile test. Therefore, the equivalent plastic strains of the central element at the fracture elongation point obtained from the numerical models were summarized in table 2-2 and compared with the fracture strain measure from thickness and width reduction of specimens (low precision). Again, model 3 gives the best prediction of the local equivalent strain to fracture. Hence, one can conclude that the model with solid elements and isotropic plasticity model can give accurate numerical prediction for the dog-bone specimen tensile tests. The reason why the shell element can not give good prediction might be that the width thickness ratio of the specimen cross-section is not big enough for a shell assumption.

One can also obtain the stress triaxiality information (negative pressure divided by effective stress) of the central point of the specimen from numerical simulation. The evolution of stress triaxiality with the elongation of the gauge section is shown in Fig. 2-18. The average triaxiality value up to fracture is about 0.345, and the triaxiality before necking is exactly equal to the analytical value 1/3. The average stress triaxiality would be used for fracture calibration together with the fracture strain.

Table 2-2 Comparison of equivalent strain to fracture of dog-bone specimen between simulations and test of dog-bone specimens

| | Model 1 | Model 2 | Model 3 | Model 4 | Measurement after test |
|---|---|---|---|---|---|
| Fracture strain | 0.12 | 0.13 | 0.48 | 0.10 | 0.53 |

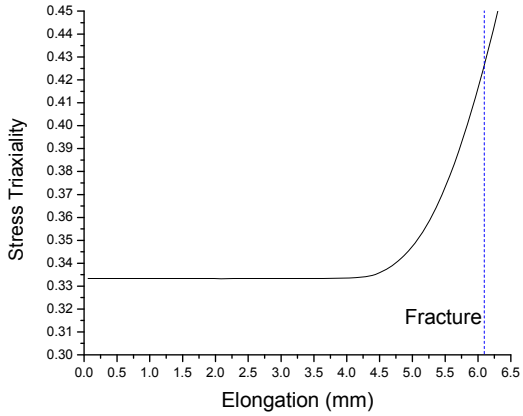


Fig. 2-18 Evolution of stress triaxiality calculated by ADINA

## 2.2 Flat specimen with cutouts

The flat specimen with cutouts was used to obtain additional point for the calibration of the ductile fracture model of our aluminum sheets. The geometry of the specimen is shown in Fig. 2-19. The initial stress triaxiality in a tensile test of this specimen can be easily controlled by changing the diameter of the cutout contour. The geometry of the specimens in this project gives an analytical initial triaxiality of 0.52. Two FE models were set up in ADINA with 4-node shell elements and 8-node solid elements respectively. With the symmetric conditions, one only need to build a 1/4 model of the gauge section with shell elements and a 1/8 model of the gauge section with solid elements. Fig. 2-20 and Fig. 2-21 shows the deformation and equivalent plastic strain contour of these two models at the fracture elongation point.

Based on the studies in section 2.1, only isotropic material model was used for the simulations hereafter, and the true stress strain curve in Fig. 2-6 was adopted. The mesh edge length of both models is 1mm. 5 through thickness Gauss integration points were used in the shell element model. The effect of the through thickness integration point number will be discussed in section 3.

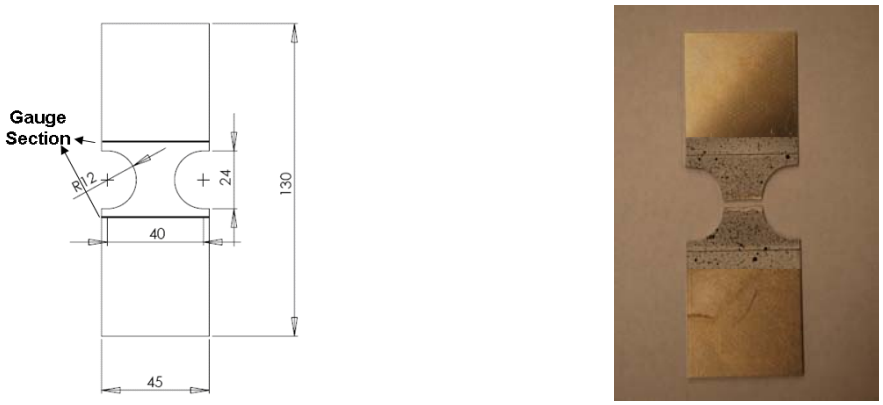


Fig. 2-19 Geometry of flat specimen with cutouts

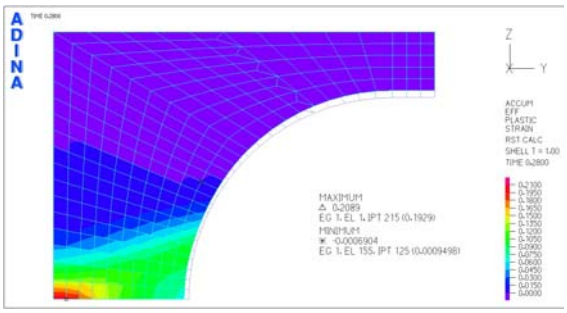

Fig 2-20 Deformation and strain output at fracture elongation point of shell element model

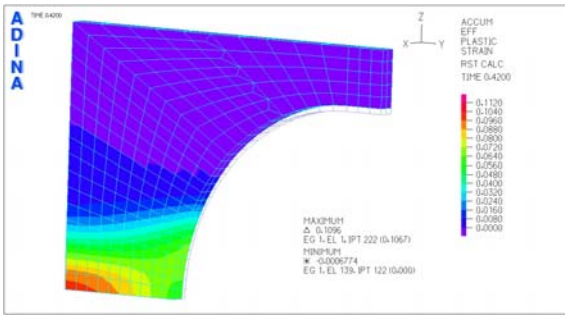

Fig 2-21 Deformation and strain output at fracture elongation point of solid element model

The load displacement responses and the experimental results were compared in Fig. 2-22. Apparently, the shell element model result correlates with experimental result better. For this specimen, crack also initiate at the center point of the specimen, so the equivalent plastic strains to fracture of the central elements of the two models were obtained from the ADINA models and are shown in table 2-3 together with the fracture strain measured after test. The shell element model gives a better prediction of equivalent strain to fracture than the solid element model.

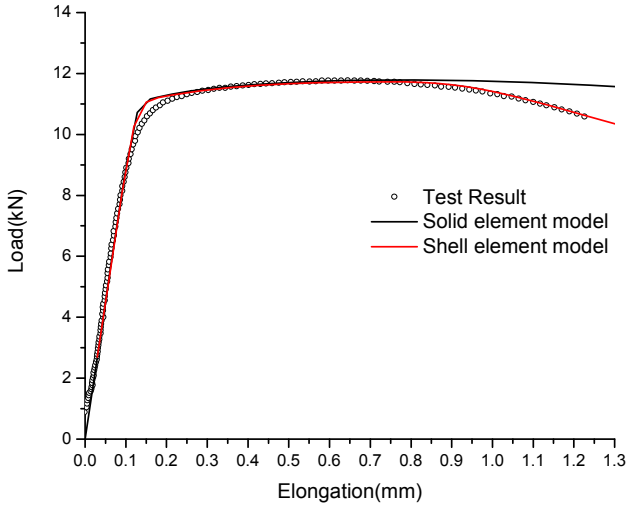


Fig. 2-22 Comparison of the load-elongation curves between FE models and test

Table 2-3 Comparison of equivalent strain to fracture between simulations and test

| | Shell Model | Solid Model | Test Measurement |
|---|---|---|---|
| Fracture strain | 0.21 | 0.13 | 0.25 |

The evolution of stress triaxiality with the elongation of the gauge section of this specimen calculated by the shell element model is shown in Fig. 2-23. The average triaxiality value up to fracture is about 0.51, and very close to the analytical value 0.52. The average stress triaxiality would be used for fracture calibration together with the fracture strain.

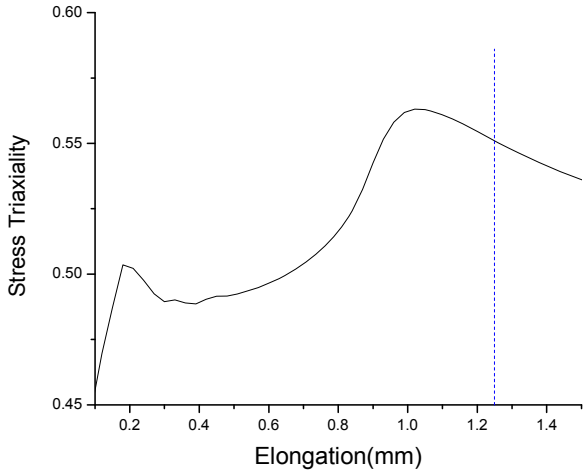


Fig. 2-23 Evolution of stress triaxility of the flat specimen with cutouts

## 2.3 Flat grooved plane strain specimen

Another type of specimen for the fracture calibration tests is the flat grooved specimen, which can provide a plane strain condition in the uniaxial tensile test. The geometry of the specimen and a tested specimen is shown in Fig. 2-24. Two FE models were set up in ADINA with 4-node plane strain elements and 8-node solid elements respectively. With the symmetric conditions, one only need to build a 1/4 model of the gauge section with plane strain elements and a 1/8 model of the gauge section with solid elements. Fig. 2-25 and Fig. 2-26 show the two models.

The load displacement responses and the experimental results were compared in Fig. 2-27. For this specimen, crack also initiate at the center point of the specimen, so the equivalent plastic strains to fracture of the central elements of the two models were obtained from the ADINA models and are shown in table 2-4 together with the fracture strain measured after test using digital image correlation method.

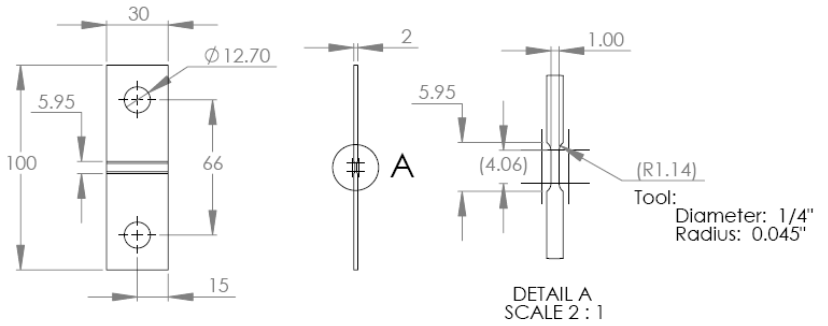


(a) Geometry of flat grooved specimen

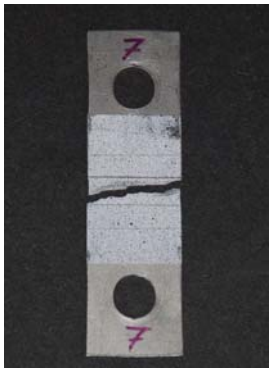

(b)A tested specimen

Fig. 2-24

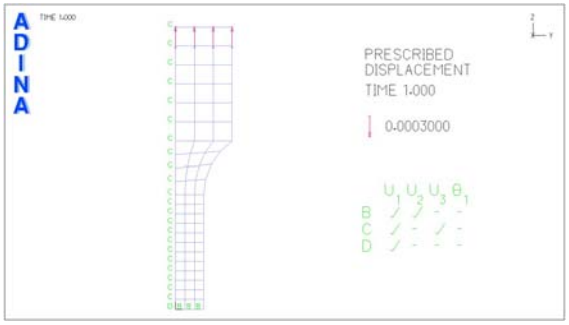


Fig. 2-25 Plane strain element model

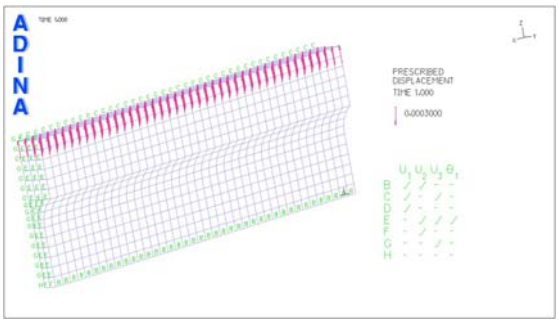


Fig. 2-26 Solid element model

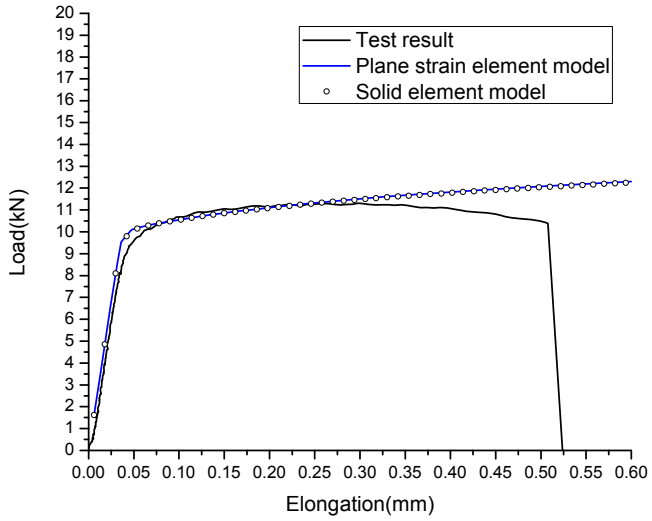


Fig 2-27 Comparison of the load-elongation curves between FE models and test of plane strain specimen

Table 2-4 Comparison of equivalent strain to fracture of plane strain specimen

| | Plane Strain Model | Solid Model | Test Measurement |
|---|---|---|---|
| Fracture strain | 0.139 | 0.138 | 0.20 |

From Fig. 2-27 and table 2-4, one can see that plane strain element and solid element model give almost identical prediction of load-displacement response and local strain at the center point of the specimen. However, using plane strain elements can greatly reduce the number of elements, and thus save CPU time. Fig. 2-28 demonstrate that the strain in x direction is almost zero, so the plane strain element is good enough to modeling tension test of this specimen.

The evolution of stress triaxialities with the elongation of the gauge section of the plane strain specimen calculated by two models are shown in Fig. 2-29. The average triaxiality value up to fracture is about 0.572, and very close to the analytical value 0.577. The average stress triaxiality would be used for fracture calibration together with the fracture strain.

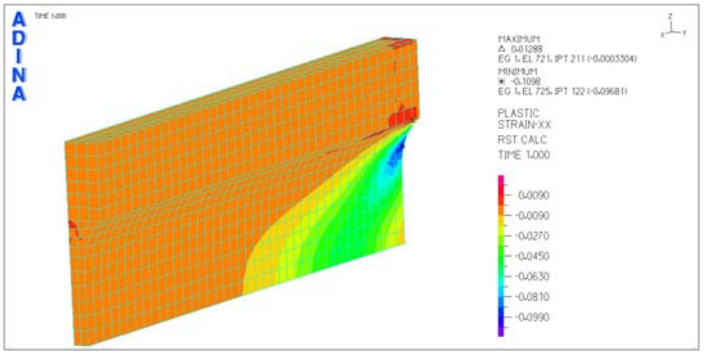


Fig. 2-28 The band plot of the strain in XX direction

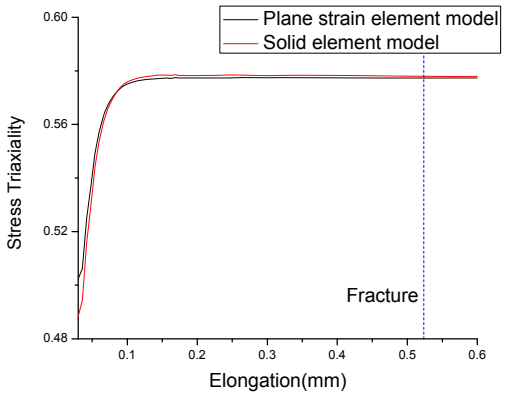


Fig. 2-29 Evolution of stress triaxility of the flat grooved plane strain specimen

## 2.4 Punch indentation tests on circular disks

This test provides information on fraction under the equi-biaxial state of stress. The most highly stressed point is located at the apex of the dome where the components of radial and circumferential stress and strain are equal to each other. The disk specimens were secured to the 100mm diameter die by a heavy flange with 8 bolts. The radius of the hemi-spherical punch was 45mm. The load-displacement characteristics were recorded in the tests. The measured displacement to fracture in our case was 27.4mm. The tests were interrupted right after formation of nearly straight crack shown, as shown in Fig. 2-30.

Accordingly, a FE model of this test was built in ADINA with 4-node axisymmetric elements, which is shown in Fig. 2-31. The mesh edge length is 1mm. The edge nodes of the disk model were fixed at all degree of freedom, the center nodes of the disk model were given a symmetric boundary condition, and the punch surface was given a prescribed downward displacement. The contact surface on the punch was modeled as rigid, and the friction coefficient is set to 0.01. The pressure/displacement mixed interpolation function was used for this model to get better stress triaxiality prediction, the difference between displacement-based and u/p mixed element will be discussed in

section 3. The time step was set to 0.005s. The deformation and the effective strain distribution of the disk were shown in Fig. 2-32.

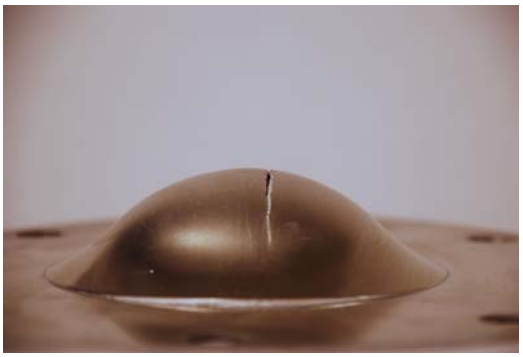

Fig. 2-30 A view of the fractured disk

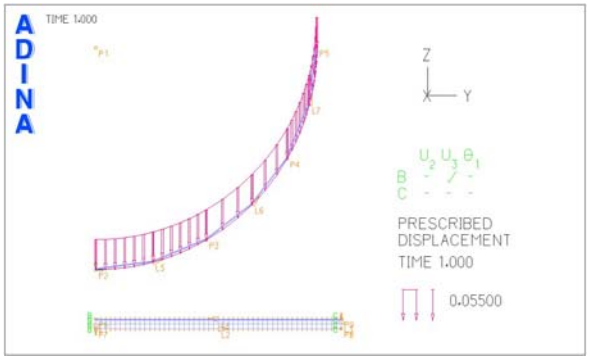


Fig 2-31 Numerical model of the punch test

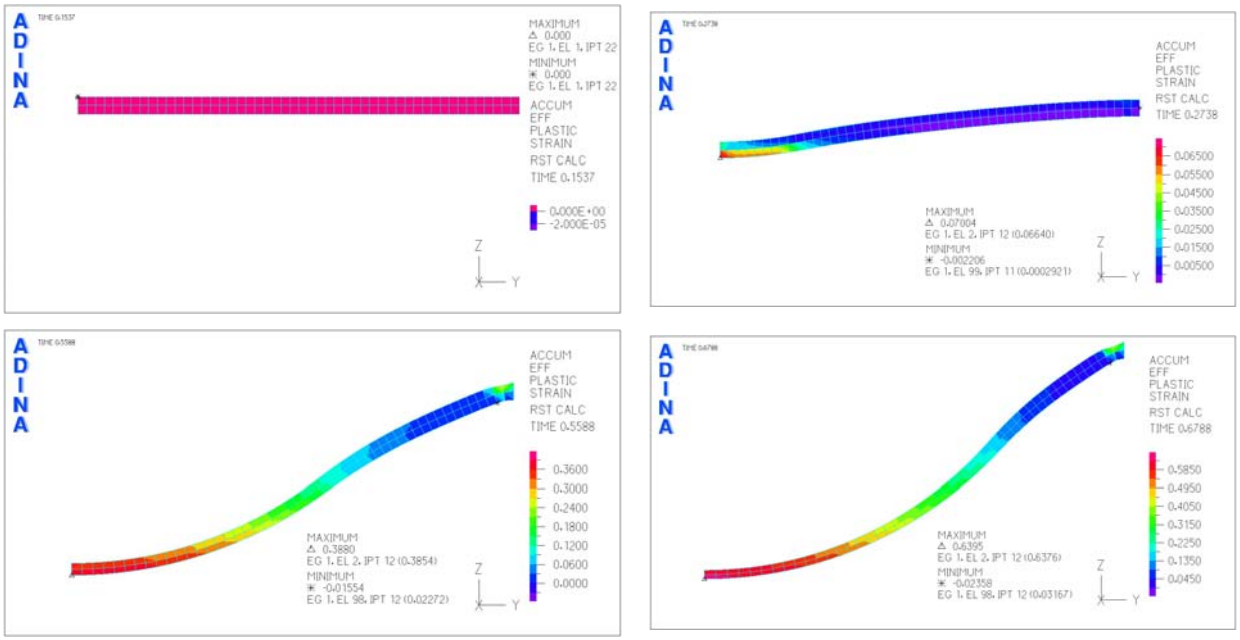


Fig. 2-32 Deformation and distribution of the disk specimen calculated by ADINA

The force displacement response can be obtained by plotting the reaction force on the punch and the displacement of the punch. The comparison of the force displacement response between simulation and test result is shown in Fig. 2-33. There is an excellent agreement of the measured load-displacement curve with the numerical model. Also, the history of the effective strain and stress triaxiality of the outer element at the apex of the dome was shown in Fig 2-34, from which one can obtain the equivalent strain to fracture of this specimen and the average stress triaxiality up to fracture of the fracture initiation point (apex of the dome). For the case of our aluminum sheet, the calculated fracture strain is 0.63, which is very close to the strain value 0.69 from the measurement of thickness reduction after test. The average triaxiality value up to fracture is about 0.65, and very close to the analytical value 2/3. The average stress triaxiality would be used for

fracture calibration together with the fracture strain 0.63.

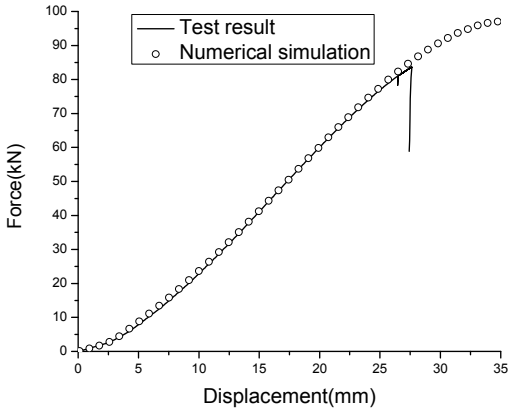


Fig.2-33 Comparison of the force displacement response of a punch test between test result and simulation output

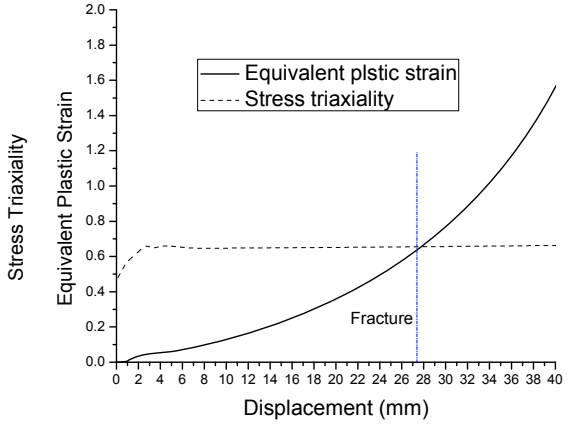


Fig. 2-34 Evolution of equivalent plastic strain and stress triaxiality at the fracture initiation point

## 2.5 Ductile fracture calibration using simulation results

As all the numerical simulations of calibration tests has been performed and validated by experimental results, a fracture locus of our aluminum sheets can be calibrated with the simulation results. Table 2-5 shows all the fracture points obtained from the numerical simulation.

Table 2-5 Fracture points obtained from numerical simulations

| Point | Specimen Type | Stress Triaxiality | Fracture Strain |
|---|---|---|---|
| 1 | Dog-bone | 0.345 | 0.48 |
| 2 | Flat with cutouts | 0.51 | 0.21 |
| 3 | Flat grooved | 0.572 | 0.14 |
| 4 | Punch indentation | 0.65 | 0.63 |

A Mohr-Coulomb fracture criterion was used to calibrate the fracture locus of this aluminum sheet. The form of this fracture criterion in the space of fracture strain and stress triaxiality is as followed:

$$\bar{\varepsilon}_f = \left\{ \frac{A}{c_2} f_3 \left[ \left( \sqrt{\frac{1+c_1^2}{3}} \cdot f_1 \right) + c_1 \left( \bar{\eta} + \frac{f_2}{3} \right) \right] \right\}^{-\frac{1}{n}} \tag{2-3}$$

where the functions $f_1$ , $f_2$ and $f_3$ are defined as

$$f_1 = \cos\left\{ \frac{1}{3} \arcsin\left[ -\frac{27}{2} \bar{\eta} (\bar{\eta}^2 - \frac{1}{3}) \right] \right\}$$

$$f_2 = \sin\left\{ \frac{1}{3} \arcsin\left[ -\frac{27}{2} \bar{\eta} (\bar{\eta}^2 - \frac{1}{3}) \right] \right\} \tag{2-4}$$

$$f_3 = c_3 + \frac{\sqrt{3}}{2-\sqrt{3}} (1-c_3)(\frac{1}{f_1} - 1)$$

This fracture criterion is a function of equivalent strain to fracture $\bar{\varepsilon}_f$ in terms of the average stress triaxiality $\bar{\eta}$ up to fracture. A and n are the material parameters in Eq. (2-1). This criterion has 3 calibration parameters $c_1$,$c_2$ and $c_3$. Hence, points 1, 3 and 4 in table 2-5 were used to calibrate the 3 free parameters, while point 2 was used to validate the accuracy of the fracture locus. The calibrated fracture locus is shown in Fig. 2-35. One can see that the calibrated fracture locus can predict the fracture strain at point 2 (flat specimen with side cutouts) with good accuracy. Therefore, this fracture locus can be implemented into the FE codes to predict ductile fracture during calculations.

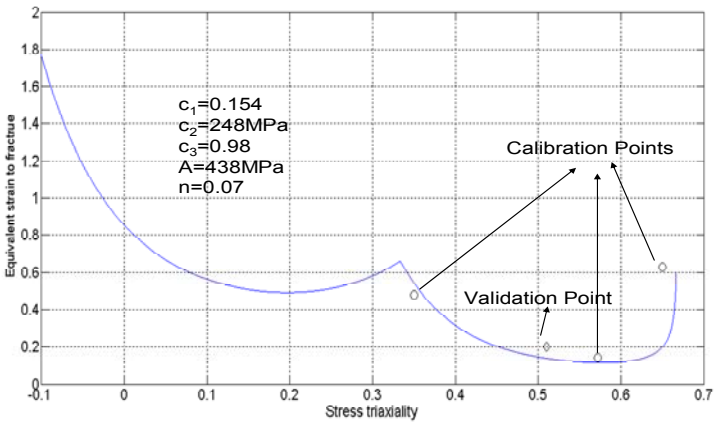


Fig.2-35 Calibrated fracture locus of our aluminum sheets with numerical results

# 3. Parametric Study of Some Numerical Simulation Parameters

To predict the initial crack position accurately, the local strain and stress triaxiality are very important to the fracture identification. However, some parameters may affect the local strain/stress significantly, such as number of integration points (NIP) through thickness, element type, mesh size and so on.

Several finite element models were built based on the benchmark models in section 2 to study these effects. The force-displacement response, effective strain and stress triaxilality history at the initial crack position were compared and analyzed.

## 3.1 Effect of Number of Integration Point through thickness (NIP)

This study is based on the shell element model of the flat specimen with cutouts. The benchmark model in section 2.2 is with 5 integration points though thickness, and the Gauss integration was used. Two more shell element models of the flat specimen with cutouts with 2 and 3 through thickness integration points respectively were built in ADINA.

As is shown in Fig. 3-1, as the NIP through thickness of shell elements increases, the load-elongation response predicted by the numerical model is closer to the experimental results. From Fig 3-2 and 3-3, one can see that the local strain and stress triaxiality at the crack initiation point (the center of the specimen) predicted by the 2 NIP model are much lower than the 5 NIP model, which has shown good accuracy in section 2.2. Hence, if shell elements are used for numerical simulations of similar problems, at least 5 through thickness integration points should be employed.

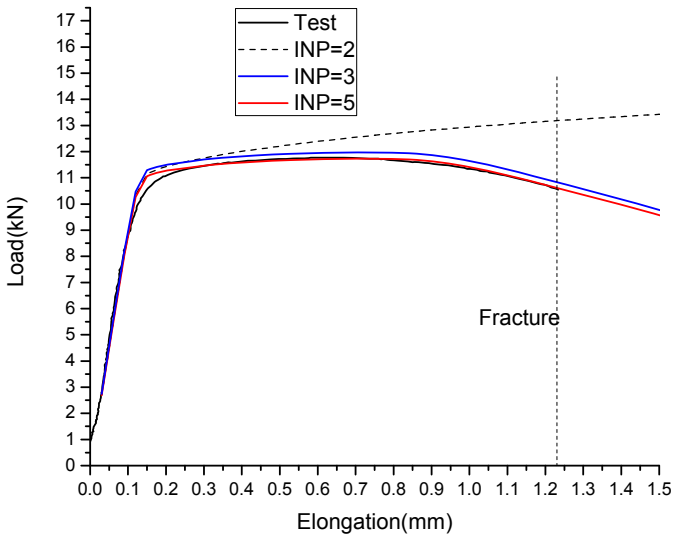


Fig. 3-1 Load-elongation responses of three models with different NIP through thickness

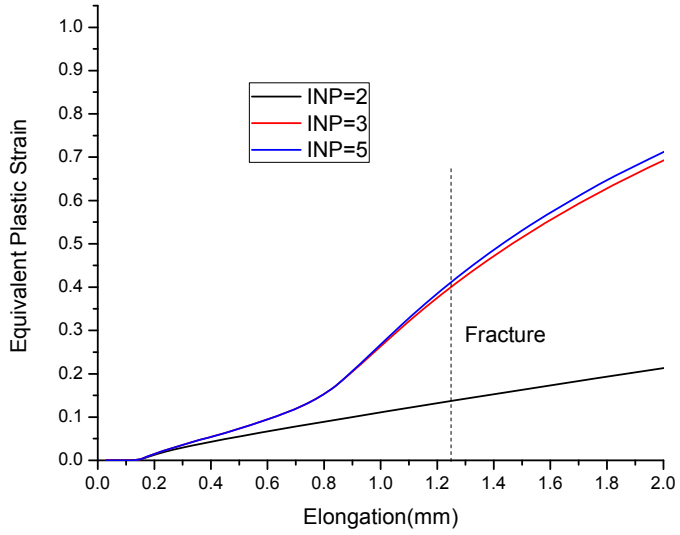


Fig. 3-2 Strain history at crack initiation point of three models with different NIP through thickness

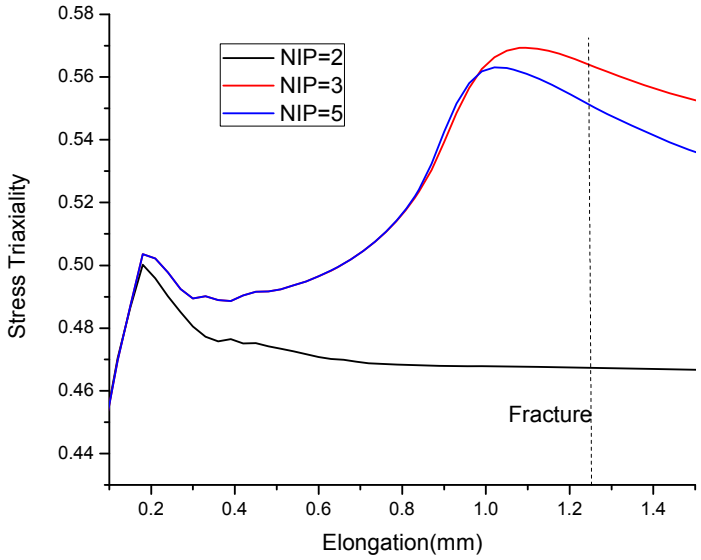


Fig. 3-3 Stress triaxiality history at crack initiation point of three models with different NIP through thickness

## 3.2 Effect of element type

This study is based on the model of punch indentation tests in section 2.4. Three different models with different element types and interpolation formulations were

compared in this section, displacement based 4-node element, mixed 4/1 and 9/3 u/p element.

From Fig.3-4 and Fig. 3-5, one can see that the force-displacement response and local strain evolution at the crack initiation point (the apex of the dome) are not affected much by the element type. However, as is shown in Fig. 3-6, the displacement based element can not predict the stress triaxiality well, because the analytical stress triaxiality value should be 2/3 in this test. Since stress triaxiality is a normalized pressure, the low accuracy triaxiality prediction is due to the unreasonable pressure distribution and magnitudes predicted by the displacement-based elements, as is shown in Fig. 3-7. The pressure distribution calculated by mixed u/p elements are much more accurate, as is shown in Fig. 3-8.

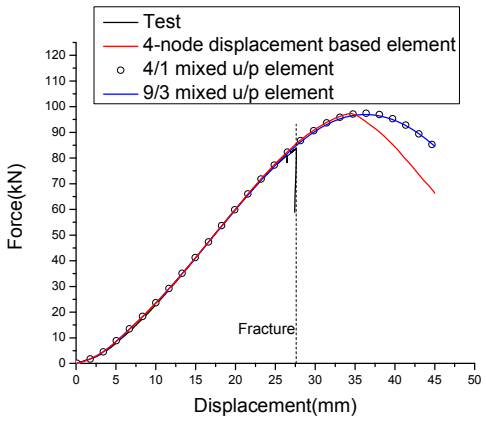


Fig. 3-4 Force-displacement responses of 3 models with different element types

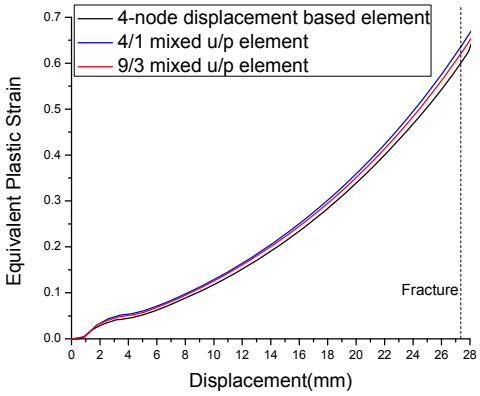


Fig. 3-5 Equivalent plastic strain evolution at crack initiation point of 3 models with different element types

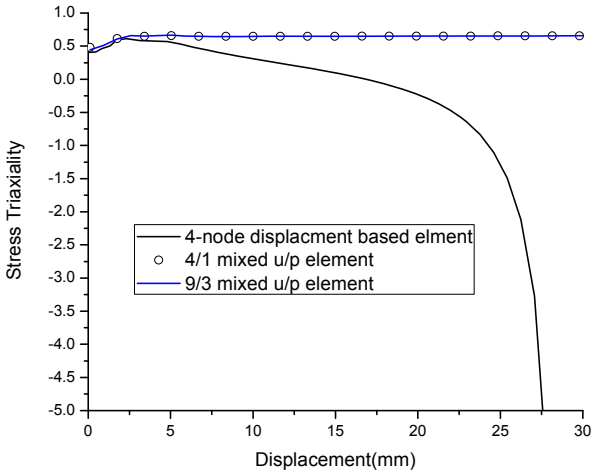


Fig. 3-6 Evolution of stress triaxiality at crack initiation point of 3 element types

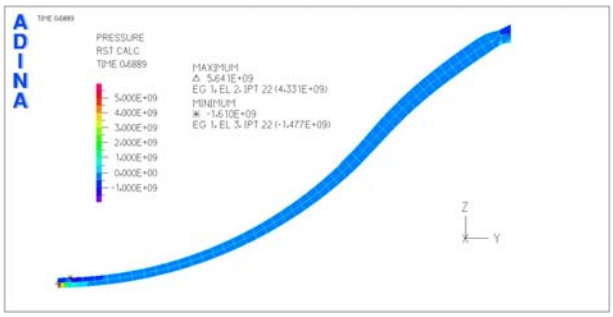


Fig. 3-7 Pressure distribution of the model with 4 node displacement based elments

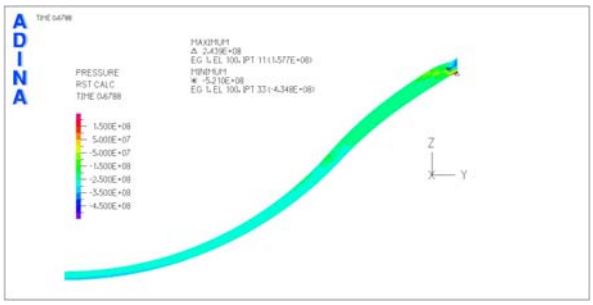


Fig. 3-8 Pressure distribution of the model with 9/3 mixed elements

## 3.3 Mesh size effect

This study is based on the model of punch indentation tests in section 2.4. Three different models with different mesh sizes were built, as is shown in Fig. 3-9, and the force-displacement responses, local strain and stress triaxiality history at the crach initiation point (the apex of the dome) were compared and studied. The 3 different mesh edge length studied in this section was 1mm, 0.5mm, and 2mm. The 4/1 mixed u/p elements were employed in all three models.

Fig. 3-10 and 3-11 show that the force-displacement response and stress triaxiality predicted by the numerical models become closer to the experimental result or analytical result as the mesh goes finer. As is shown by Fig. 3-12, the local strain seems to be larger as the mesh edge length is smaller in the early stage, but it reach convergence finally. Hence, the finite element model is convergent as the mesh becomes finer.

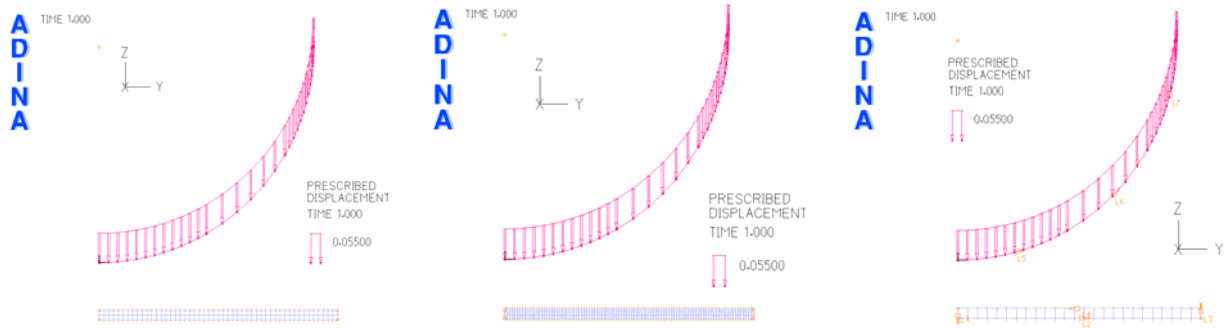


(a)Mesh edge length=1mm (b)Mesh edge length=0.5mm (c)Mesh edge length=2mm

Fig. 3-9 Three models with different mesh size

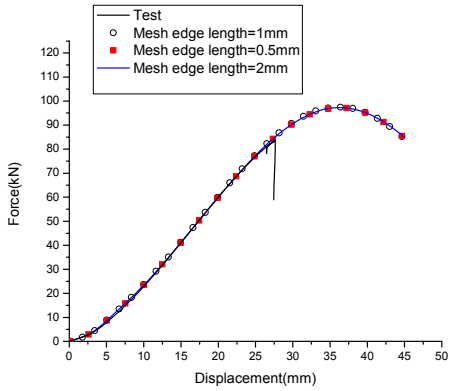


Fig. 3-10 Force-displacement responses of 3 models with different element size

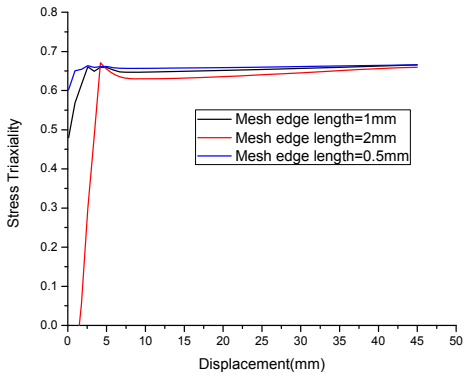


Fig. 3-11 Evolution of stress triaxiality at crack initiation point of 3 models with different element size

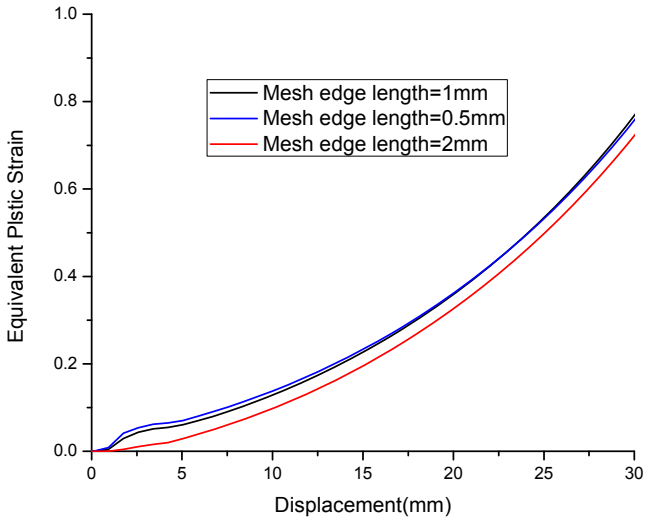


Fig. 3-12 Equivalent plastic strain evolution at crack initiation point of 3 models with different element size

## 4. Conclusions

In this project, four types of specimens made from our aluminum sheets were tested in the lab to investigate the fracture characteristics of this material. At the same time, corresponding finite element models were built to simulate the fracture calibration tests. Most suited model for each test was determined after comparisons and analysis, and the fracture locus of this material was calibrated with the simulation results. Moreover, a brief parametric study was performed to evaluate the effect of several FE parameters on the numerical simulation results. Main conclusions are shown as followed:

1) Finite element model can simulate the physical problems very well. Suited FE models can predict the load-displacement responses, local strain and stress with good accuracy.
2) Selection of element type and modeling strategy should depend on the geometry and boundary conditions of the physical problem. For this project, one should choose solid elements for dog-bone specimen, shell elements for flat specimen with cutouts, plane strain elements for flat grooved specimen, and axisymmetric elements for the punch indentation test.
3) Number of integration points (NIP) through thickness has a great effect on the strain and stress distribution of shell elements. Once the through thickness stress gradient is involved in a physical problem, such as necking or bending, a larger NIP through thickness should be employed.
4) The u/p mixed element can predict the pressure distribution and magnitude much more accurate.
5) The FE models in this project are convergent. As the mesh becomes finer, both the load-displacement response and local stress/strain output become closer to experimental results or analytical values.

2.094 Finite Element Analysis of Solids and Fluids II
Spring 2011